Int. J. Therm. Sci. (2000) 39, 852–870

S1290-0729(00)01195-9/REV

Review paper

Heat, mass and momentum transfer in coating formation by plasma spraying

P. Fauchais [a], A. Vardelle [b]*

[a] *SPCTS UMR 6638, Faculté des Sciences, 123 Avenue Albert Thomas, 87060 Limoges cedex, France*

[b] *SPCTS UMR 6638, ENSIL, 16 Rue Atlantis, 87068 Limoges cedex, France*

(Received 25 July 2000, accepted 7 September 2000)

Abstract — The plasma jets produced by d.c. spray torches exhibit unusual properties: high flow velocities (up to 2 500 $m{\cdot}s^{-1}$), high temperatures (up to 14 000 K), steep temperature and velocity radial gradients (up to 10^7 $K{\cdot}m^{-1}$ and 5.10^5 s^{-1}) and low gas density ($1/30$ to $1/50$ that of the cold gas). They are laminar in their core and turbulent in their fringes. When they exit the torch nozzle, the resulting vortices coalesce inducing an engulfment process of the ambient gas with large scale eddies entraining bubbles of cold gas. The latter do not mix instantaneously with the plasma due to the high density difference. Mixing occurs after the heating of the cold inclusions. In addition, the plasma jets are continuously fluctuating in length and position because of the continuous movement of the arc root on the anode wall at frequencies ranging between 3 and 20 kHz. This results in a sort of piston flow. In plasma spraying, the solid particles are injected in the plasma jet through an injector set downstream or upstream of the nozzle exit. In this injector, particles collide between themselves and the injector wall. Therefore, they have trajectory and velocity distributions at the injector exit. It results in a dispersion of their trajectories within the jet. The flow rate of the powder carrier gas has to be adjusted to give the particles about the same momentum as that of the plasma jet at the injection point. The large difference between particle and flow velocity can induce convective movements within the molten droplets resulting in a continuous renewing of the liquid material at the particle surface. For metal or alloy particles sprayed in air this internal movement brings about a high oxidation rate enhanced by the presence of atomic oxygen in the jet. Particles impact on the part to be covered at velocities between 150 and 300 $m{\cdot}s^{-1}$. The liquid material spreads out from the point of impact and forms a lamella called "splat". The flattening time is below a few μs and splat solidification generally starts before the flattening process is completed. The next particle that impacts a few tens of μs later, flattens on already solidified particles. The piling up of a few splats forms a pass in less than one millisecond, then, the next pass is deposited a few seconds later. The thickness of a pass varies between 3 and 60 μm. The flow and heat phenomena during the impact and solidification processes control the microstructure and thermo-mechanical properties of coatings. The build-up of a coating in plasma spraying is a multiscale problem with time scales ranging between microseconds and seconds and length scales ranging between a few micrometers and a few hundred micrometers or more. Therefore, models and experiments deal with either the formation of splats or the piling of layers. This paper will review what is our present knowledge of the modeling and measurement of the transient phenomena involved in the various subsystems of the plasma spray process: jet formation, particle injection, particle heating and acceleration and coating formation. © 2000 Éditions scientifiques et médicales Elsevier SAS

1. INTRODUCTION

Plasma spraying is part of thermal spraying that is a group of processes in which finely divided metallic and nonmetallic materials are deposited in a molten or semi-molten state on prepared substrates [1, 2]. The heat source is a plasma jet produced by a direct current (d.c.) arc (99 % of the market) or a radio-frequency (RF) discharge. In most cases (about 95 % of the plasma spray market), d.c. plasma guns are working in air at atmospheric pressure. This process is called Atmospheric Plasma Spraying (APS). RF discharges [3] and some d.c. arcs work in a controlled atmosphere chamber filled with a neutral gas (mostly argon) either at atmospheric pressure or slightly over [4] or under a soft vacuum (20–50 kPa) [5]. The main advantage of controlled atmosphere is the avoidance of the oxidation of metal powders and substrates during the spray process.

The solid particles introduced in the plasma jets are accelerated and melted or partially melted. There is no limitation in the melting temperature of the sprayed material provided the material melts, i.e. the difference between melting temperature and decomposition or evapo-

* Correspondence and reprints.
armelle@ensil.unilim.fr

ration temperatures is higher than 300 K. Upon impact on the substrate, the droplets form splats which solidify in a few μs [6]. Therefore, the next droplet impact on already solidified splats. The coating, resulting from the layering of splats which thickness is between 0.8 and a few μm, has a lamellar structure and its properties are different from those of the same bulk material [1, 2].

The base-material and coating combination can be tailored to provide resistance to heat, wear, erosion and/or corrosion, as well as unique sets of surface characteristics. Coatings can also be used to restore worn and mismachined parts to original dimensions and specifications. At present, plasma spraying has moved from coating technology to materials processing technology with a growing importance [7].

As a matter of fact, this deposition process is governed by momentum, heat and mass transfer phenomena and the reliability and reproducibility of coating properties depend on the control of these phenomena.

This paper will present what is our knowledge in the heat, mass and momentum transfer involved in plasma spraying. It will address successively plasma sources, particles in flight and upon impact and coating formation. The subject will be limited to the description of atmospheric plasma spraying.

2. PLASMA SOURCES

2.1. Description and involved phenomena

The d.c. plasma spray torches generally use a blown arc configuration with a hot thoriated tungsten cathode. The latter is either of stick type (*figure 1a*) or button type (*figure 1b*).

With stick-type cathodes, the electric power levels are below 60 kW and the plasma-forming gas flow rates below 120 slm (in most cases, in the order of 40–60 slm); the thermal efficiency of the gun ranges between 40 and 60 %. With button-type cathodes, the electric power levels reach 250 kW and gas flow rates 300–400 slm; the thermal efficiency of the gun is about 70–75 %. This higher thermal efficiency results from the gas flow rate inducing higher arc voltage. The anode nozzle internal diameter ranges between 6 and 8 mm for stick-type cathodes and 8 mm for button-type ones. The specific enthalpy is a few $MJ \cdot kg^{-1}$, the plasma velocity at the nozzle exit is up to 2 000 $m \cdot s^{-1}$, but subsonic, and the temperature up to 14 000 K.

In the nozzle, the arc stretches between the tip of the stick-type cathode or the center of the button-type one, and the water-cooled anode wall. The working gas is introduced either axially or with an additional swirl component. For guns with button-type cathodes, it is the only way to center the arc. The plasma column expanding from the cathode arc root is stabilized by the water-cooled wall of the anode-nozzle and plasma-forming gas flow. During plasma column expansion, a part of the plasma-forming gas is entrained in the arc column. The arc strikes the anode when the cold boundary layer close to the anode wall has been heated enough [8, 9]. With the flow superimposed to the arc, the arc attachment at the anode is unsteady. The connecting column, between the arc column and anode surface, crosses the cold boundary layer and is pushed downstream by the flow. Its 3-D transient motion is determined by the relative magnitude of the forces acting on it: drag force from the flow and Lorenz forces due to self-magnetic field (*figure 2*).

The magnitude of arc motion is determined by the thickness of the cold boundary layer which in turn depends on the plasma-forming gas composition, the arc current controlling the diameter of the plasma column

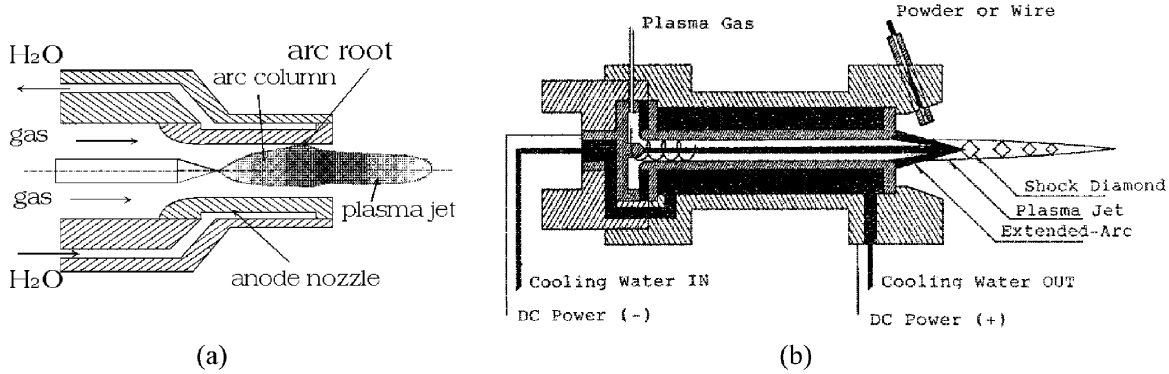

Figure 1. D.c. plasma spray torches with (a) a stick type cathode, (b) a button-type cathode.

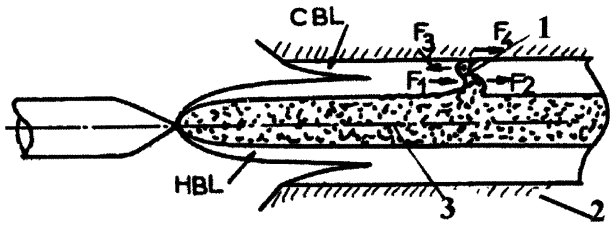

Figure 2. Schematic of the forces acting on the connecting column (1) between the anode wall (2) and the plasma column (3). $\vec{F}_1$: drag force of the "cold" flow in the boundary layer, $\vec{F}_2$ and $\vec{F}_3$: $\vec{j} \times \vec{B}$ forces due to the self induced magnetic field, $\vec{F}_4$: friction force at anode surface, HBL: Hot Boundary Layer, CBL: Cold Boundary Layer.

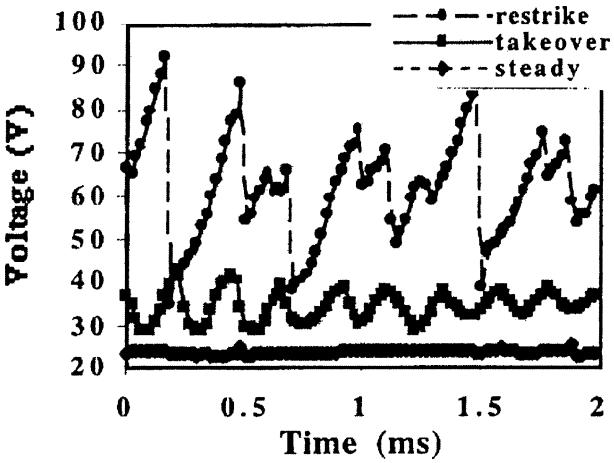

Figure 3. Typical voltages due to arc root fluctuations at the anode [10]: (a) steady mode, (b) takeover mode, (c) restrike mode.

and the torch anode-nozzle internal diameter [10]. The connecting column lengthens and increases its voltage up to a value corresponding to the breakdown voltage resulting in a short-circuit with a new re-arcing. Three modes can be observed for arc voltage fluctuations:

(1) "steady mode"; it is rather detrimental for the anode lifetime and is obtained for too high arc currents relatively to the anode-nozzle internal diameter;
(2) "takeover mode" obtained with monoatomic gases as helium, argon and their mixture; and
(3) "restrike mode" for pure diatomic gases (hydrogen, nitrogen) or their mixtures with argon [11–15].

Figure 3 shows typical voltage traces for these different attachment modes.

In the restrike and takeover modes, the stretching–rearcing process results in a plasma bubble disconnected from the arc column when a new arc root is created (in times between 50 and 200 μs). Thus, the plasma jet is a succession of hot puffs, separated by colder domains [16, 17]. This phenomenon produces variations in the enthalpy levels of the jet and, therefore, in the heating rates of particles. That is why works are in progress to design new plasma torches with longer arcs (higher voltage) and, correlatively, less voltage fluctuations [18].

2.2. Characterization of plasma jets

2.2.1. General remarks

Spray d.c. plasma jets are characterized by temperatures up to 14 000 K, velocities up to 2 200 $m \cdot s^{-1}$, high heat fluxes (up to 10^{10} $W \cdot m^{-2}$ in the plasma core), reduced dimensions (<10 mm), steep temperature gradients (up to 10^7 $K \cdot m^{-1}$) as well as velocity gradients (up to $5 \cdot 10^5$ s^{-1}) and important fluctuations in the 0.1 ms range. Therefore, measuring methods have to be nonintrusive, at least in the plasma core, and time and space resolved.

2.2.2. Temperature

The most popular [19, 20] technique for plasma temperature measurement is emission spectroscopy. Monochromators are now equipped with CCD detectors, cooled with liquid nitrogen and computer-controlled. They allow a very fast treatment (a few ms) of the recorded data especially for Abel's inversion. Temperatures higher than 8 000 K are determined from atomic line absolute intensity, assuming equilibrium, which is questionable in the jet fringes. The method can exhibit fast response times (∼μs) and requires a few seconds to scan a plasma jet. It allows the comparison of plasma jet cores as a function of gun operating conditions. In the plasma jet plume, emission spectroscopy based on molecular spectra ($3\,000 \leq T \leq 10\,000$ K) can be used but it is by far more complex and time-consuming with only time-integrated ($t \sim 10$ ms) signals [19, 20]. Enthalpy probes coupled to a mass spectrometer (probe diameter ∼ 3 mm) allow the determination of the gas enthalpy and, thus, temperature knowing the gas composition [21, 22]. However, this method is intrusive and the obtained temperatures are Favre-averaged values while that obtained by emission spectroscopy are time-averaged ones.

More sophisticated techniques such a Rayleigh scattering [23] or Coherent Anti-Stokes Raman Spectroscopy (CARS) are also used [24].

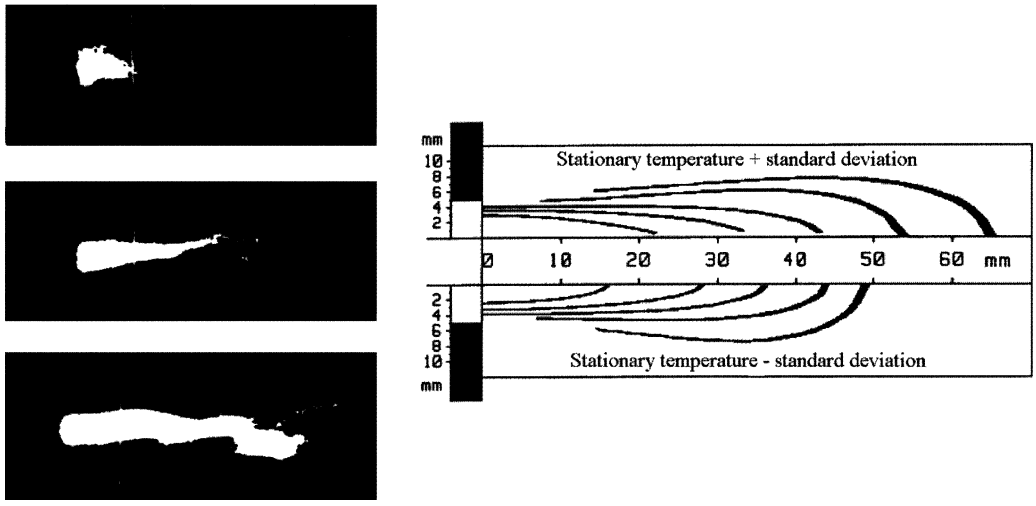

(a) (b)

Figure 4. (a) Pictures of a d.c. plasma jet taken with a shutter time of 10^{-4} s, (b) temperature measured with ArI 738.3 nm line $\pm$ standard deviation (measuring time $\sim$100/ms). ArH_2 (45–15 slm) plasma jet; nozzle i.d. 10 mm, $I = 632$ A, $V = 61$ V, thermal efficiency of the gun 56%.

2.2.3. Velocity

In the plasma core, optical methods based on the propagation of the light fluctuations due to arc root fluctuations can be used [25, 26] while in the plasma plume, enthalpy probes coupled with mass spectrometer can be utilized [21, 22].

2.2.4. Imaging

The use of CCD cameras with nitrogen-pulsed laser illumination [27] or high speed video systems [28] allows the follow-up of the transient behavior of plasma jets.

2.2.5. Results

Figure 4 illustrates the measuring problems. *Figure 4a* represents pictures of a d.c. plasma jet taken with a shutter time of 10^{-4} s at a frequency of 24 Hz. It shows the fluctuations of the jet due to the arc root fluctuations. *Figure 4b* represents the same plasma jet with a time-averaged (100 ms) temperature distribution, assuming a cylindrical symmetry of the jet, as observed by the eye through a black window. In the latter figure, arc root fluctuations are accounted for by adding and subtracting a standard deviation to the mean value.

CARS measurements [24] performed in an argon d.c. plasma jet flowing in air have shown an interesting phenomenon: the air bubbles entrained by the plasma jet are not mixed with it but slowly heated. Nitrogen temperature within the bubbles varies in the plasma core between 2 000 and 4 000 K while emission spectroscopy performed on ArI lines at the same location indicates temperatures over 9 000 K. This has been confirmed by spectroscopic measurements showing that the oxygen contained in the entrained air bubbles is completely dissociated while nitrogen is not [29].

2.3. Plasma gas properties

Depending on the material to be sprayed and the plasma gun used, the plasma-forming gas are pure Ar, Ar–He, Ar–H_2, N_2–H_2 or Ar–He–H_2. The various spray gases contain always a heavy gas such as argon or nitrogen to achieve a high gas momentum. The latter helps to push and stabilize the arc root downstream in the anode nozzle, and accelerate the particles without using a too high gas flow rate.

2.3.1. Equilibrium

(a) Plasma forming gas mixtures. Thermodynamic and transport properties of plasma-forming gases mixed with air (surrounding air entrained in the plasma jets) have been calculated at equilibrium [30–33]. They are characterized by strong nonlinear variations. Thermal plasmas exist only when the electron molar fraction x_e is over 0.01. This corresponds to a temperature in the order of 8 000 K for Ar, N_2, O_2 and H_2 and 13 000 K for pure He. Below these temperatures, the electrical

conductivity σ_e is too small. However, it has to be noted that a high value of σ_e in the plasma, for example, at 14 000 K, is two orders of magnitude smaller than that of a copper wire.

When dissociation (between 3 000 and 5 000 K for H_2 and O_2, 6 000 and 8 000 K for N_2) or ionization (between 8 000 and 16 000 K for Ar, N, O, H and 12 000 and 26 000 K for He) occur, the enthalpy and sound velocity exhibit strong variations. Correlatively, the plasma specific heat at constant pressure c_p and thermal conductivity κ exhibit peaks, the reactional part of κ being linked to c_p. The highest values of κ are obtained over 3 000 K for H_2 and 12 000 K for He. Thus, plasma gas mixtures contain very often one of these two gases to enhance the heat transfer to particles. The plasma jet density is, depending on temperature, 20–40 times lower than that of the cold gas. Sound velocity depends strongly on the molar mass of the mixture and for spray d.c. plasma jets, depending on gas composition and temperature, it ranges between 1 600 and 2 800 $m \cdot s^{-1}$.

When $x_e > 0.03$, long-range interactions prevail and plasma viscosity decreases, i.e. over 10 000 K for Ar, N_2, H_2, O_2 and 14 000 K for He. The addition of helium to other plasma-forming gases shifts the temperature of the maximum viscosity to higher temperature values.

The calculation of diffusion coefficients is very complex. A method has been proposed by Murphy [33] combining the multi-diffusion coefficients that does not entail any loss of accuracy provided the gas mixture is assumed to be at equilibrium. Such calculation makes it possible to explain the behavior of the plasma column when adding light gases to the plasma-forming gas as the diffusion of hydrogen to the column fringes [34] due to its low mass and that of helium to the jet axis due to its much higher ionization potential [35].

According to temperatures encountered in plasma jets, the radiation energy can be easily neglected [30]. However, it becomes important as soon as metals are vaporized. For example, at 4 000 K the radiated energy of an Ar plasma seeded with 1 mole % of Fe is equivalent to that of the pure argon plasma at 10 000 K. Moreover, calculations become difficult because the plasma is no more optically thin and effective radiation has to be calculated. This is achieved by using the method of effective emission coefficients assuming that the plasma is an isothermal sphere and calculating the net emission coefficient as a function of the temperature and radius of the plasma [36, 37]. Another method is that of the mean absorption coefficients [38, 39]. It is based on the curving of the spectrum in some interval strips in which the total absorption coefficient is constant for a given temperature within each strip. The limits of the intervals are mainly defined by the sudden jumps of the evolution of the continuum absorption coefficient due to the electronic structure of species. The jumps correspond to photon energies equal to ionization or dissociation energies. As for the net emission coefficient calculations, it points out that radiation absorption is mainly due to resonance lines situated in the far UV for plasma-forming gases and in the visible for metals.

(b) Plasma gases mixed with the surrounding atmosphere. In most cases plasma jets flow in air and the main problem is to determine the local composition, thermodynamic and transport properties of the mixture. For transport properties, the problem becomes rapidly time-consuming because they depend on the interaction potentials of all pairs of species. For a mixture containing K species, $K(K-1)/2$ collisions have to be considered. For Ar–H_2 mixture, $K = 6$ but for an Ar–H_2–air mixture, $K = 20$! To limit the calculation time, mixing rules are used [40]. They give a good agreement with the full calculation of the transport properties of the mixture. It should be noticed that, in plasma sprays, the plasma jet core is laminar but with limited dimensions while the jet fringes and the plume are turbulent. In the latter, the turbulent transport properties are more important than the molecular properties.

2.3.2. Nonequilibrium flows

When a cold gas is injected in a plasma or when the plasma is close to a wall, the plasma is no more at equilibrium. It can be characterized by two kinetic temperatures [30]: the temperature of electrons T_e and that of heavy species T_h proportional to the mean kinetic energy of the particles through the Maxwellian distribution. Once the composition is known, transport properties [30] except diffusion [41] can be calculated. The plasma composition is established using methods derived from equilibrium calculations: Multitemperature Saha Equation (MSE) [42] or Excitation-temperature Saha Equation (ESE) [43]. These methods are as fast as equilibrium calculations but their results, when compared to kinetic calculations, are questionable [44–46]. When starting from simple gases such as N_2 or H_2, kinetic calculations are three orders of magnitude longer [46] which makes the flow calculation almost impossible. Recently a new pseudo-equilibrium method has been proposed; it considers only the low activation energy reactions and keeps all species present in the kinetic calculations. It is at least two order of magnitude faster. This method gives the same results as those of kinetic calculations for N_2

and H_2 [46]. Works are in progress to check this method for complex mixtures.

2.4. Flow modeling

2.4.1. Current-carrying plasma

Over the past two decades, various works related to the modeling of d.c. arcs and plasma jets have been reported in the literature. For establishing a complete model of an arc, it is mandatory to include the electrode region as well as the transition from the plasma to the electrode surface. Many works have been devoted to these phenomena that are summarized in the paper of Heberlein [47]. They show that strong deviations from kinetic equilibrium prevail in these regions. Even if the hot cathodes working in a steady state are now rather well characterized, contradicting evidence still exists. In particular, the transport of material issued of multi-component cathodes, i.e. the diffusion of the emission material in a tungsten matrix and the re-deposition of the material after evaporation, should be clarified. The dissolution of the plasma gas in the molten emitting spot is not understood. But the big challenge is the description of the phenomena at the anode wall. This description has to be dynamic and three-dimensional and involve the numerous parameters affecting the arc–anode interaction.

That is why most models have been restricted to two-dimensional situations. Local thermodynamic equilibrium (LTE) and electrical neutrality are assumed to prevail in the whole computational domain, even near the electrode walls. The classical equations are used: mass, momentum, energy and current density conservation, Ohm's law and Maxwell's equations for electric potential, the magnetic field being calculated from the current density with the help of the Ampere's theorem. The plasma is assumed to be optically thin and a global radiation term, function of temperature, is introduced in the energy conservation equation. The flow is assumed to be noncompressible and either laminar, which is certainly the case in the plasma column but not necessarily in the fringes, or turbulent with a low Reynolds k–ε model to account for the laminar core [48]. The effect of the swirl, if any, can also be taken into account [49–52]. In this 2-D treatment for the anode, a potential surface orthogonal to the axis is considered which position can be determined by using the Steenbeck minimum principle. This principle implies that the arc seeks the position that requires the minimum voltage for maintaining it [53]. Beside the necessity to include cathode phenomena in the model, the 2-D model implies that the entire gas flow has to pass through the current connection to the anode but this assumption is totally unrealistic. Therefore, it is not surprising that the agreement between measurements and calculation is not bad for temperature (*figure 5*) but not very good for velocity distribution.

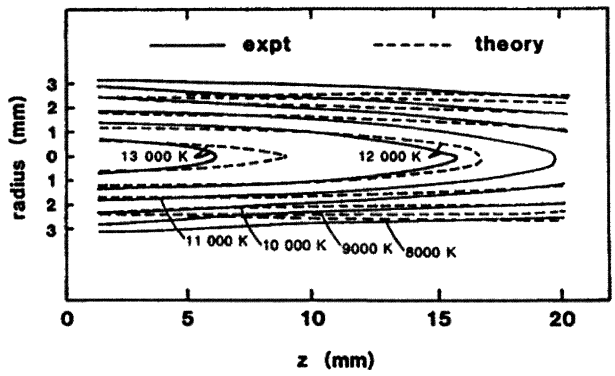

Figure 5. Experimental (solid line) and theoretical (dashed line) temperature contours for a plasma torch working with a nozzle i.d. 6 mm, 400 A, 33.2 V, 30 slm Ar (torch exit at $z = 0$).

3-D transient modeling of the arc column has been reported [48, 54] but without detailed consideration of the electrode regions and the modeling of the transient behavior of the arc is still pending.

2.4.2. Plasma jets

A range of models has been proposed [55–62] to calculate the plasma jet temperature and velocity distributions. These models start with the results of the calculations described in the previous section or calculate temperature and velocity distributions at the nozzle exit matching with the plasma gas flow rate and enthalpy. The codes consist in momentum and thermal energy equations for the multi-component fluid mixture, continuity equations for each component of the mixture taking into account the mixing with the surrounding atmosphere but usually neglecting chemical reactions, and state relations for an ideal gas mixture with temperature-dependent specific heat, enthalpy and transport properties. The models are 2-D or 3-D [60–62]. However, 3-D modeling is mandatory to study the perturbation of the plasma jet by the carrier gas. LTE is generally assumed except in the LAVA codes of Chang et al. [60, 61]. Turbulence effects are taken into account using either a standard or a modified k–ε turbulence model as the low Reynolds k–ε model. In general, the equations are parabolic but they can also be elliptic [57, 60–62].

The k–ε model is, as a matter of fact, not well adapted to d.c. plasma jets, as shown by Pfender and his coworkers [24, 63]. The large velocity difference between

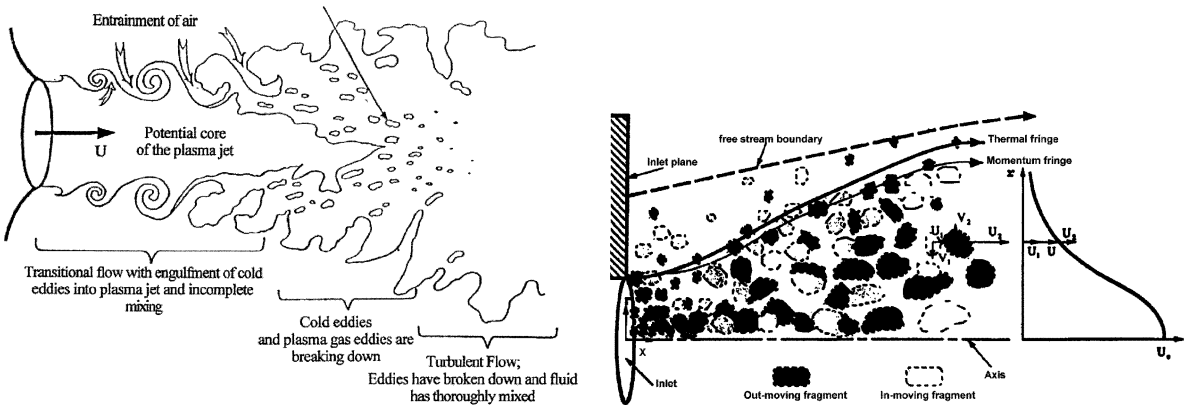

Figure 6. (a) Main regions of a transient plasma jet [24]. (b) Boundaries of the computational domain and exchange of U-momentum [66].

the plasma jet and its surrounding atmosphere results in a large-scale engulfment of the outside gas (*figure 6a*). It has been corroborated by shadography, CARS spectroscopy measurements [24] and probe sampling of the plasma jet [64]. A multiphase model for turbulent flow could reproduce these effects as proposed by Spalding [65]. Such a model has been developed by Huang et al. [66] for an argon plasma jet flowing into an argon stagnant environment. The plasma jet is considered as a two-fluid mixture consisting of hot, out-moving fragments and cold, in-moving fragments as shown schematically in *figure 6b*. The obtained results for the axial distributions of temperature and velocity are in good agreement with measurements.

At last, the piston flow induced by the anode arc root fluctuations should also be taken into account as measurements show its effect on the surrounding air entrainment within the first twenty millimeters of the jet [29].

3. PARTICLES IN FLIGHT

3.1. Description of involved phenomena

The solid particles are injected locally in the plasma jet through one or two injectors thanks to a carrier gas [67]. The injection geometry (injector design, position and angle with the torch centerline) and mode (inside or outside the nozzle) control to a large extent the distribution of particle trajectory in the plasma jet and, therefore, their acceleration and heating. In most cases, the injector is orthogonal to the jet axis either inside the anode-nozzle (downstream of the arc root) or outside it. Typical injector internal diameters range between 1.5 and 2 mm and their positioning has to be achieved with a precision better than 0.1 mm.

The powders used in plasma spraying may have very different morphologies depending on the manufacturing process. Even if powders manufactured by various processes may appear to be equivalent with respect to chemical composition and particle size distribution, they will have different treatment in the flow and the properties of the resulting coatings [68–71] will vary. The particle characteristics that affect their treatment in the gas flow are mainly their shape that controls their flowability, their density that affects their acceleration and heating, and their purity.

Plasma-sprayed powders have distributions typically in the range 10–45 μm for ceramics and 45–90 μm for metals [1, 2]. During their pneumatic transport through the injector, they collide between themselves and the injector wall. These collisions are responsible for the particle jet divergence at the injector exit. This divergence is specially marked for particles with diameters below 20 μm and it will result in a broad distribution of trajectories within the plasma jet. The dispersion of particles by the flow turbulence enhances this phenomenon [67].

When the particles penetrate the plasma jet core, they are first heated and accelerated. Then, in the plasma plume, they decelerate and slowly cool down. Particles treated in d.c. plasma flows have a residence time in

the millisecond range and receive a heat flux as high as 10^8 W·m^{-2} [63]. As a result of the high gradients in the plasma jet, particles which follow different trajectories, will have different accelerations and heatings. The larger and denser particles are more resistant to the flow drag force and spend more time in the plasma jet, which is favorable for the plasma spray process. However, for large particles of low density and low conductivity materials, the rate of heat conduction in the particles may be too slow to ensure a homogeneous heating and melting during the residence time of the particles in the plasma jet. Particles can react in flight with the plasma gas or surrounding gas which mixes with the plasma jet, and undergo chemical reactions, decomposition and evaporation [72]. In addition, the large difference between particle and flow velocity may induce convective movements within the molten droplets, at least those which melting temperature is below 2 300 K [73]. This results in a continuous renewing of the liquid material at the particle surface. For metal or alloy particles sprayed in air this liquid movement brings about a high oxidation rate enhanced by the presence of atomic oxygen in the plasma flow.

3.2. Measuring devices

The characteristics of plasma-sprayed coatings depend directly on the parameters of the particles arriving at the substrate. Therefore, over the years, a number of different techniques have been developed to measure the distributions of particle size, velocity and temperature [19, 20, 74–76]. The determination of particle temperature is generally based on the measurement of the thermal radiation emitted by the particles in two or more wavelengths or color bands. Their velocity is measured either by laser Doppler velocimetry [74] or transit timing techniques [77, 78]. In the latter, the velocity is deduced from the time of passage of the particle between two apertures or focused laser spots. The particle size is deduced either from the intensity of the particle thermal radiation using an absolute intensity calibration [78] or from the phase shift between two or more light signals scattered by a particle crossing a laser-focused beam and collected at various angles with the original laser beam [79]. Most of these techniques are single-particle methods and the distribution and standard deviation of particle parameters are obtained from the observation of a large number of individual particles. However, some techniques can be considered as "ensemble techniques" as they measure simultaneously the properties of a large number of particles and yield directly an average value of these parameters. Up to now, these ensemble techniques could only provide information on particle temperature but very recently an ensemble technique has been developed for particle velocity [80].

Imaging techniques can also be used to monitor the shape and position of the centroid of the particle spray jet as well as the density of hot particles, or determine particle temperature and size from the intensity of the light signal and velocity using a double exposure technique [81, 82]. The incorporation of a laser in the measuring device makes it possible to determine the number of "cold" particles as well as their size and velocity [81].

Some techniques, commercially available, can now be used in production environment to have on-line control of the spray process. They are generally based on the measurement of the thermal radiation emitted by the particles and do not use any additional light sources. They allow the measurement of particle velocity, temperature and size distributions and can help to produce coatings in a more consistent manner day after day [83].

Finally, some measurement systems based on absorption spectroscopy have been developed to investigate the evaporation of the particles in plasma flow. They allow the determination of the population of metal atoms in various locations in the jet and in the vapor cloud surrounding individual particles [84].

3.3. Modeling

The modeling of particles acceleration and heating in the flow use the conventional equations for droplet motion in flows and heat transfer. However, some effects specific to thermal plasma environment must be taken into account. The main effects are due to the high temperature gradient prevailing in the boundary layer surrounding the particles, strongly varying plasma properties, non-continuum conditions, thermophoresis, turbulent dispersion, evaporation and possible chemical reactions on the particle surface [85, 86]. Moreover, when the Biot number related to particles is higher than 0.01, the heat transfer in the particle has to be taken into account as the temperature gradient within the particles can be large [87]. The models based on the heat conduction equation are generally one-dimensional and allow the tracking of the melting, evaporation and possible resolidification front in a particle. However, recent works have shown that the large difference in velocity between the flow and particles can induce convective movements inside the particles [73].

In the modeling of the plasma spray process, the conditions of particles injection in the flow govern the particle trajectory distribution and, therefore, their treatment. Thus, these conditions must be as realistic as possible and involve the particle size, injection velocity and direction distribution at the injector exit. The description of powder injection that implicates a stochastic aspect is still a challenging problem [67, 88].

Most of the codes used for the modeling of plasma spraying consider the particles as Lagrangian entities and can deal with several particle types. A statistical processing of the calculated data (particle velocity, size, melting state) makes it possible to determine the distributions of particle parameters in various cross sections of the plasma jets and particle impact pattern at substrate position. These 2-D or 3-D codes differ by the way they take into account the mixing of the plasma jet with the surrounding gas, the transient or stationary behavior of the jet, the thermodynamic and transport properties of the gas mixture, the possible reactions between the gaseous species, the heat conduction inside the particles, their evaporation and the chemical reactions on the particle surface [61–63]. They use generally the k–ε models as turbulence model and corrective coefficients for particle drag and heat transfer to take into account varying plasma properties and noncontinuum effects.

4. SPLAT FORMATION

4.1. Description of the involved phenomena

The production of coatings with closely controlled and reproducible properties requires a broad understanding of the phenomena occurring after impact of the particles on the substrate. Significant progress has been made in the understanding of splat formation and coating building and numerous theoretical and experimental investigations have been reported, e.g., [94–96]. However, many important questions remain such as the phenomena resulting in the splashing of droplet upon impact, the change in splat shape with substrate temperature, and the effect of substrate surface contamination or oxidation on splat shape.

When a particle hits the substrate, the sudden deceleration causes a pressure build-up at the particle-surface interface; the high pressure inside the particle forces melted material to flow laterally or ductile material to deform. The liquid spreads outward from the point of impact and forms a “splat”. The arresting of spreading results from the conversion of particle kinetic energy into work of viscous deformation and surface energy. Solidification constraint (when the solidification front is advancing from the substrate surface fast enough to interact with the liquid during spreading) and mechanical constraint (due to the roughness of the substrate surface) can interfere with the flattening process [89].

The spreading kinetics of the impacting droplets govern the splat shape and thickness, the ability of the sprayed material to fill existing voids and the quality of contact between the splat and the underlying layer, thereby controlling local cooling rate and overall heat transfer. The efficient heat extraction by the substrate results in a high cooling rate (10^6–10^8 K·s^{-1}) through both liquid and solid phases, leading in turn to undercooling and rapid solidification [90, 91].

The process of splat formation depends on the velocity, size, molten state, chemistry and angle of impact of the droplets onto the surface. It is also subject to the surface topography of the substrate, its temperature and reactivity. This process determines both microstructural (crystalline phases, crystallite size) and macroscopic characteristics (porosity, adhesion) of the coating. In addition, as the thermal contraction of splats is constrained by the underlying solid, tensile stress is developed during deposition. This quenching stress can be relieved by various mechanisms such as microcracking, plastic yielding, creep and so on [92, 93]. As a result, thermal-sprayed coatings have a characteristic microstructure of lamellae, pores and cracks. Metal coatings may also include oxides formed during particle flight up to the substrate or after impact.

4.2. Experimental observation of splat formation

The simplest way of getting information about splat formation is the observation of isolated lamellae on substrates using optical microscopy, scanning electron microscopy or atomic force microscopy. The geometry of the splats can be also measured using a surface profilometer.

This observation makes it possible to investigate the role that a specific preparation (chemistry and roughness) of the substrate surface and its temperature play on the splat geometry. It also enables linking the latter with the average thermal and kinetic energy of the particles prior to impact using measuring systems that allow the measure of in-flight particle parameters, e.g., [97, 98]. These parameters are controlled by the operating conditions of

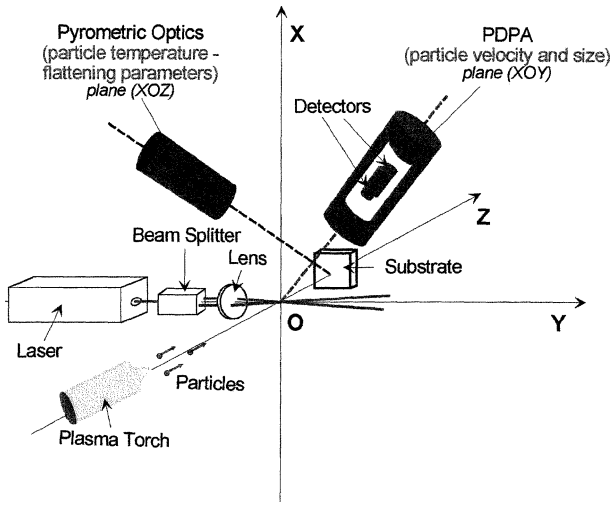

Figure 7. Scheme of the experimental set-up using a pyrometer and a PDPA for the study of particle impact (from [104]).

the gun and the injection conditions of the sprayed material. In this way, relationships between process parameters and splat formation can be determined. However, such studies do not permit a comprehensive understanding of splat formation involving the impact process and the solidification phenomena that are the keys to a control of coating building. This requires to determine, for one particle, its size, temperature and velocity before impact and to follow the flattening and time–temperature evolution of this droplet on the substrate.

Experimental data on the droplet impact under thermal spray conditions are scarce due to the difficulty to get accurate data on a micrometer-size droplet. Experiments have been carried out for millimeter-size droplets impinging on a surface at low velocity so that the dimensionless numbers characteristic of the impact process are similar to those prevailing in thermal spraying. However, the importance of the involved phenomena such as the degree of undercooling, nucleation delay and contact resistance, is not the same in systems differing in two or three orders of magnitude [95]. Recently, two techniques based on the detection of the thermal radiation emitted by the particles have been developed. The first uses a pyrometer focused onto the substrate to measure the parameters of a particle prior to impact and determine its temperature evolution during the flattening and cooling stages on the substrate [99–102]. The light from the particle is focused onto the tip of an optical filter covered with an optical mask opaque to the near-infrared radiation except for 3 slits. On a glass substrate, the splat diameter evolution during its cooling can also be measured independently of the thermal radiation using the attenuation of a laser-diode beam [102]. The second technique consists of a pyrometer focused onto the substrate and a phase Doppler particle analyzer [103, 104]. The latter makes it possible to measure the velocity of the particle and its size, independently of its temperature, while particle temperature before and during impact is measured using a two-wavelength optical pyrometer. The principle of the measurement system is shown in *figure 7*.

These techniques enable an estimation of the flattening time, flattening degree ξ (ratio of the splat diameter to the original particle diameter) and cooling rate of the impinging particle. They have shown that, in plasma spraying, the flattening time is generally less than 1 μs; ξ varies between 2 and 6 and is larger for metals; cooling rate ranges between 10^6 and 10^8 K·s^{-1}.

Imaging devices are also under development for the visualization of particle impact in thermal sprays [105].

4.3. Modeling

For splat formation, analytical models have been proposed for droplets impacting at 90° onto a smooth surface. They express the flattening degree ξ as a function of dimensionless groups characteristic of the impact and spreading process: the Reynolds number (*Re*) that quantifies the viscous dissipation of the inertia forces, the Weber number (*We*) that expresses the conversion of the kinetic energy into surface energy and a heat transfer parameter, the Peclet number (*Pe*), used to characterize the solidification rate. The most popular analytical model provided by Madejski attempted to include viscous force, surface tension and crystallisation kinetics [106]. Simplifying by assuming that the spreading is complete before solidification becomes significant and that the surface tension effects can be neglected, gives $\xi = 1.2941(Re + 0.9517)^{0.2}$. Surface tension effects are generally acknowledged to be minor under thermal spray conditions, except perhaps for droplet size <10 μm and at the end of the flattening process. For $Re > 100$, this equation yields $\xi = 1.2941Re^{0.2}$. Similar expressions with different constants have been established from analysis analogous to that of Madejski [107, 108] or from the fit of the results of numerical modeling [109].

Over the last years, various numerical studies have dealt with the impact of a thermal-sprayed particle on a smooth surface, e.g., [109–113]. The majority assumes a two-dimensional geometry and the most advanced solve the flow equations taking into account convective, viscous and surface tension effect. They track the material deformation during impact and involve the solidification

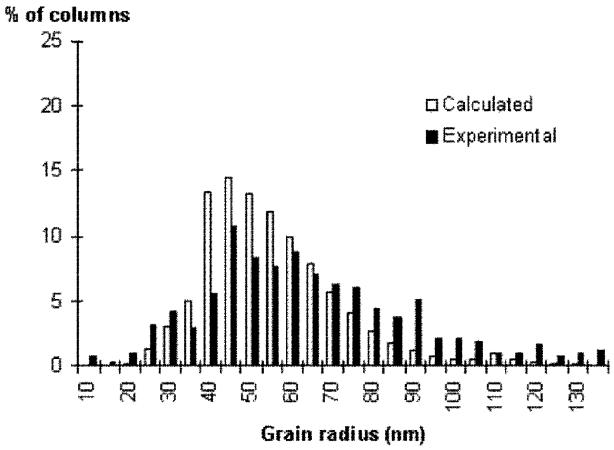

Figure 8. Comparison between calculated and experimental grain size distributions of an alumina splat on an alumina substrate at 300 °C (from [116]).

process and heat interaction of the droplet with the underlying surface through an interfacial thermal contact. Such models enable the evaluation of the effect of particle parameters at impact on splat formation. However, they cannot predict the breakup or splashing of the particles onto the surface. Recently, Mostaghimi et al. have proposed a three-dimensional modeling of the droplet impact incorporating a model of droplet splashing based on Rayleigh–Taylor instability theory [114]. This model showed that for an alumina droplet thermal-sprayed on a cold surface the particle breaks in the form of a corona of fluid around the splat. This result is supported by experimental evidence [102]. However, phenomena other than Rayleigh–Taylor instabilities can play a role in the splashing at impact. The last 3-D calculations of Bussmann and Mosthagimi show that splashing can result from solidification during the spreading process [114].

The numerical models of splat formation assume, as a general rule, that the thermal contact resistance between the splat and the substrate is very low (10^{-7}–10^{-8} $m^2 \cdot K \cdot W^{-1}$). This is probably the case at the beginning of the flattening but might not be the case at the end of it. Besides, experimental data [100], one-dimensional heat transfer models of splat cooling [115] have shown the drastic influence of the value of the interfacial thermal resistance on splat cooling. These models that involve melt undercooling, nucleation and crystal growth have also shown that high degree of undercooling can be achieved under thermal spray conditions: both interface contact and undercooling may induce significant delay in nucleation [95, 116]. These heat models enable also the prediction of the size distribution of the grains in ceramic splats characterized by an essentially columnar grain structure as shown in *figure 8*.

4.4. Effect of the particle parameters at impact and substrate condition on splat formation

The observation of isolated splats collected on smooth substrates shows that they can exhibit very different shapes, from perfect disks to jagged or disintegrated lamellae [94, 95]. Their morphology governs the quality of contact with the underlying layer, size and distribution of pores, quenching stresses and microstructure (crystal size, phase selection). The latter is mainly controlled by the rate of heat extraction, the direction of heat flow and splat thickness. The specific surface of splats may also affect the degree of oxide formed after impact.

The shape of splats is the result of intricate interactions between the parameters of the particles at impact and the condition of substrate. The control of splashing is still a puzzling problem.

Obviously, an increase in particle velocity at impact causes an increase in the kinetic energy of particle, and a rise in particle temperature brings about a decrease in material viscosity. Both result in a diminishment of the splat thickness [110, 117]. Experimental works have also shown that they make splashing easier [95].

It has been observed that the temperature of the substrate plays a major role in splat formation. On smooth substrates, below a certain substrate temperature, usually called “transition temperature”, the droplets splatter into several fragments interconnected or not, while above this temperature, they retain their coherence and spread out in the form of disks. Moreover, the physical contact between the splats and the underneath surface is improved on hot substrates. Different explanations have been proposed related to thermal effects or surface chemistry. This phenomenon has been attributed to a delay in nucleation when the temperature of the splat–substrate interface is maintained at a certain temperature ensuring that the material remains liquid during splat formation [72, 118]. It is also supposed that, at lower substrate temperature, part of the liquid “splinters” away because the spreading of liquid is impeded by the solidified part of the splat. This interpretation is consistent with recent 3-D modeling of particle impact. Another explanation is based on the contamination of the substrate surface by condensates and adsorbates [119, 120]. They vaporize and rapidly expand upon droplet impact and cause instabilities in the spreading process. Ex-

periments conducted on low-temperature substrates have shown that splat morphology changes from highly fragmented to disk-like shapes with a decrease in the level of surface contamination. Other explanations are related to wettability [121]. However, phenomena at impact are complex and these different explanations are not necessarily at variance.

The effect of substrate roughness on the flattening and cooling of droplets depends on the relative dimensions of unevenness with respect to splats. In general, the spreading of the liquid material is inhibited by an uneven surface. This causes a decrease in the flattening degree and the resulting lamellae are thicker [100].

The morphology of metal splats can also be affected by the surface oxidation of the impinging droplets and substrate [104, 117].

5. COATING FORMATION

5.1. Description of the involved phenomena

As the particle distribution within the spray jet has a Gaussian shape, the relative gun-to-substrate motion torch results in the formation of a bead which shape, on a flat substrate, is roughly Gaussian. The height of this bead depends on the torch to substrate relative velocity v_t, powder mass flow rate m_p^0 and deposition efficiency ρ_d [122]. A "pass" is formed by the overlapping of successive beads. Its thickness depends on the bead characteristics and their percentage of overlapping. Thus, a coating is built by successive impacts of particles in a molten or a plastic state on the substrate or the previously deposited layers, the next particle impacting on an already completely solidified one. Thus, coating thermomechanical properties depend not only on the way particles flatten and the resulting splats solidify and cool down, but also on the thermal history of particles layering at the same location. This fact was underlined by McPherson [123] in 1981 long before measuring devices to study splat formation and their layering were developed.

The temperature–time history of layering splats is governed by very different time-scales [124]. They are linked to the powder feed rate (2–6 kg·h^{-1}), the particle size (controlling their number per kg), the deposition efficiency (usually around 50 %), the torch/substrate relative velocity v_t (between 0.01 and 1.5 m·s^{-1}) and the time for the torch to come back at the same location usually in the 0.1–10 s range for small size parts ($d <$ 0.5 m). This time depends on the part size, v_t and the time to reverse the torch motion direction. To summarize the different time scales:

- A single splat: a particle flattens in 1–2 μs and solidifies in 2–10 μs.
- A bead: at its maximum height 3 to a few hundreds splats can be layered at the same location. For a classical powder feed rate of 4 kg, impacting particles 30 μm in diameter, a deposition efficiency of 50 %, about 3–4 splats are layered at $v_t = 1.5$ m·s^{-1} while up to 300–400 can be layered at 0.015 m·s^{-1}. Typical values between two successive impacts are between 10–100 μs while the formation of a bead occurs locally in 0.1 to 10 ms.
- A pass: the time between two successive passes is between 0.1 to a few s for small parts.

These different temperature–time histories will influence, on the one hand, the phase composition, grain size, contacts between successive splats (controlling adhesion or cohesion as well as thermo-mechanical properties) and, on the other hand, the stresses evolution within the coating which in turn can influence thermo-mechanical properties (creep, cracks, etc.).

To limit as much as possible temperature gradients within the coating and substrate during spraying, and achieve a surface temperature higher than the transition temperature T_t, substrate and coating temperatures have to be monitored during the process. In general, a preheating with the plasma torch is achieved to have the substrate temperature over T_t but with a specific temperature ramp to control the oxide layer composition and thickness [125] and the coating surface temperature is kept as constant as possible during spraying [126].

5.2. Measuring set-ups

Beside the classical characterization methods of coatings once they are sprayed (porosity, adhesion/cohesion, Young's modulus, residual stresses [93, 127]), a few methods have been developed to follow on-line certain parameters during coating generation.

5.2.1. Coating and substrate temperature

What can be measured is only a time-integrated temperature, most of the used equipments having a response time between 0.01 and 0.1 s. It means that the recorded temperature will be that of the surface of a pass. Measured temperatures being between 350 and 1 100 K, IR pyrometry is mandatory. Its advantage is also that

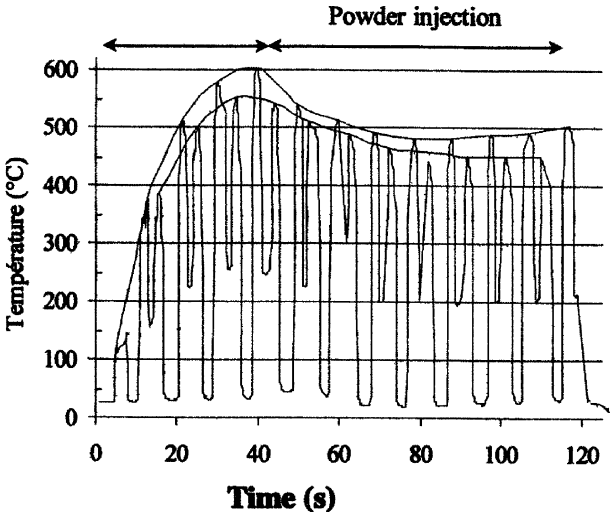

Figure 9. Time–surface temperature evolution of a $2 \times 10 \times 1\,000$ mm^3 low-carbon steel beam during its preheating and its spraying by a zirconia coating [128].

over a wavelength of 2 μm the plasma emission is rather weak. The disadvantage of such a pyrometer is that it requires a calibration for the emission coefficient which is not necessarily the same for the substrate (it depends also on its roughness) and the coating. It may also vary with the coating or substrate oxidation during spraying or preheating.

Anyhow, the pyrometer signal will be disturbed by the passage of the torch [126]. That is why, with the miniaturization of IR sensors, the best way is to install the pyrometer head on the torch and aim it out of the sprayed spot [128]. A typical example is given in *figure 9* when spraying on a beam $2 \times 10 \times 100$ mm^3 to measure the residual stresses during spraying. The surface temperature exhibits two maxima and two minima due to the fact that the sensor is fixed on the torch. For the two maxima, the highest temperature is measured when the pyrometer aims an area which has just been sprayed, the torch moving forwards with the pyrometer aimed behind it. The lowest corresponds to the backward movement, the pyrometer aiming the preceeding pass to be sprayed, i.e. in front of the sprayed spot. The two minima correspond to the torch aiming out of the beam. The lowest value is at the free extremity (the pyrometer aiming the room wall) while the highest minima correspond to the pyrometer aiming the substrate holder heated by the plasma plume. The filtered signal of the maxima is used to control the air flow rates in the cooling systems to keep the mean temperature as constant as possible during spraying.

IR cameras have also been used to monitor the temperature of large surfaces with complex geometry in order to point correctly the cooling nozzles to avoid too high temperatures in certain parts [129–131].

5.2.2. Acoustic emission during spraying

The feasibility of using Acoustic Emission Analysis (AES) as a tool for on line control of atmospheric plasma spraying has been recently demonstrated [132]. The start and end of a pass can easily be determined to get a detailed evaluation of signal to gun position relation, moreover, energy release events such as crack formation, debounding or spallation are followed.

5.2.3. Residual stresses

The main stresses in a coated substrate are due to:

- grit blasting with a compressive peak below the substrate surface [133] which can be partly relaxed during preheating, especially if the preheating temperature is close or over the recovery temperature,
- splat cooling inducing a tensile quenching stress [124, 133, 134],
- expansion mismatch resulting from the difference in expansion coefficients of coating and substrate. It increases with the temperature difference between the mean spraying temperature and room temperature.

A much better understanding of their development occurred thanks to set-ups allowing determination of their evolution during coating generation, evolution compared with simple analytical models taking into account the progressive deposition [135]. All of them are based on measuring continuously the curvature or the displacement of a rectangular beam during spraying [136–140]. They use either a mechanical sensor or a laser beam with a CCD camera. In some cases the beam is disposed on a rotating cylinder [136, 138].

A typical result is presented in *figure 10*. It shows the partial relaxation of the grit blasting stress during preheating, equivalent to a tensile stress due to the relaxation of a compressive stress, the development of quenching stresses during spraying at $T1 = 580$ °C and then at $T2 = 650$ °C. In the latter case the contacts between splats are better: $\sigma_q(T1) > \sigma_q(T2)$. A last when spraying is terminated, the temperature decrease as well as the deflection (creation of a compressive stress, the expansion coefficient of steel being higher than that of the alumina coating: $14{\cdot}10^{-6}$ K^{-1} compared to $8{\cdot}10^{-6}$ K^{-1} for alumina).

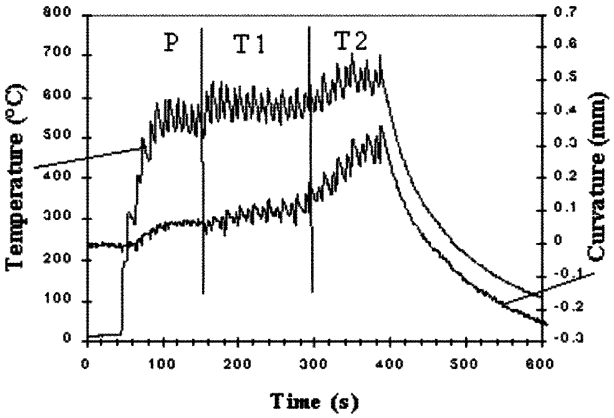

Figure 10. Time evolutions of a beam (XC 38 steel) temperature and defection when spraying alumina. *P*: preheating at 550 °C, *T*1: spraying a 250 μm alumina coating at ∼580 °C, *T*2: spraying alumina at 650 °C. Each pass is 25 μm thick [133].

5.3. Modeling

5.3.1. Thermal history of splats layering

A simple 1-D model of Haddadi et al. [134, 141] and Fauchais et al. [142] makes it possible to calculate the temperature–time history of a splat on which other splats are layering. This is illustrated in *figure 11* for the first splat of the 60th pass, each of them being made of three 1-μm thick layered splats. *Figure 11a* for alumina shows the poor reheating effect by the next impacting splats compared to what happens with zirconia (see *figure 11b*). The difference is essentially due to the diffusivity values of the two materials. It can be noted on both figures that once the three splats are layered, during the time gap between two successive passes (about 1 s) the temperature of the coating drops to a mean temperature. The latter depends on the substrate preheating temperature, cooling devices used to reduce the heat flux from the plasma jet [143] and the pass thickness. For example, when layering thick passes of oxides ($K < 20$ W·m^{-1}·K^{-1}) it is possible to achieve a columnar growth through the whole pass [141, 144]. This is made possible because the whole pass remains in a liquid state before it starts solidifying from the pass bottom.

5.3.2. Residual stresses

Commercial codes such as FEM-code ABAQUS [145] are used to simulate the thermally cycled cylindrical thermal barrier coatings [146, 147]. Of course, the results depend strongly on the creep data used for the calculation depending themselves on the residual stresses after coating. Works are in progress to adapt the 1-D analytical model taking into account progressive deposition to a 2-D situation and to couple it to the 2-D thermal history of the layering splats.

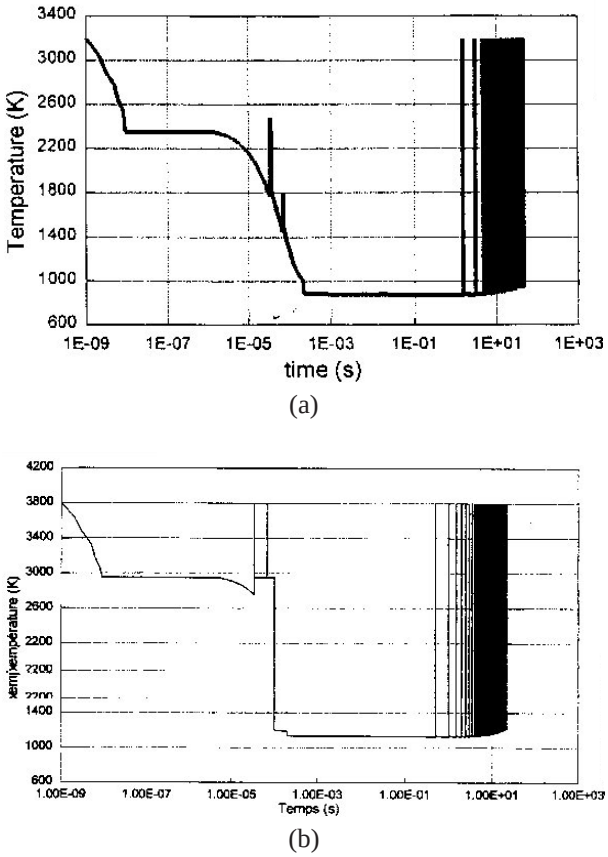

Figure 11. Temperature–time history of the first splat of the 60th pass, each pass being made of three 1-μm thick splats: (a) alumina splats, (b) zirconia splats.

5.3.3. Control of pass thickness

Coating parts with complex shape and keeping the pass thickness constant as well as the torch axis as close as possible to the normal of the part at the sprayed spot location requires the use of computerized robots. Several papers have been presented for predicting coating thickness and defining robot trajectory [148–154]. The simulation model makes it possible to use a fairly cheap way of obtaining a deposit rate from measurements and is fast enough to be suitable for optimization on complex parts.

5.3.4. Coating formation

Models related to the piling up of splats to form coatings [155–160] try to represent the coating microstructure by making predictions about the relationship between porosity or thermo-mechanical properties and process parameters. All of them require complex rules of deposition:

- First, a description of the particle on arrival with the description of each particle flattening to produce a splat which is allowed to curl up during cooling. Porosity is produced if the gap between the curled splat is not filled by subsequent splats.
- Second, a set of physically-based rules for combining the flattening events and splats layering.

Unfortunately, the predicted properties depend very strongly on the used rules and assumptions and when compared with measurements the gap is often rather large. Recently a 3-D model of free-surface flows with heat transfer, including solidification, has been used to model the build-up of a coating layer [161]. It allows prediction of the layering of a few splats (up to three layers). The results compare relatively well with pictures of the splats. Thus, it is promising but very time consuming.

6. CONCLUSIONS

During the last decade the plasma spray process has evolved from an art to a science thanks to:

- Fast cameras showing the transient behavior of plasma jets that act like a piston flow. This behavior is mainly controlled by the arc root fluctuations at the anode wall. They depend on the thickness of the boundary layer between the plasma column and the anode-nozzle internal diameter. Even if this piston flow is not taken into account in the k–ε models used to model plasma jets they give a good trend of the jet behavior with the torch working parameters. The agreement is especially good if the inlet velocity and temperature profiles are measured.
- Devices to measure in flight the key microscopic parameters: particle trajectory, velocity, temperature and diameter. It is worth underlining that such devices use more and more imaging techniques. Such set-ups have been simplified to determine the same parameters in the harsh environment of spray booths. They are now the basis of on-line monitoring of the spray process and works are in progress to transform them in on-line control with a feedback to the input macroscopic parameters (arc current, gas flow rates and composition, etc.). The modeling of in-flight particles is now well developed and the last years efforts are devoted to the statistical treatment of the particles. It allows the account for the trajectories distribution due to the collision of the particles with the injector wall and between themselves as well as for the turbulent effects in the jets. Particle modeling has also shown that the drastic difference between the plasma jet and molten particle velocities induces convective movements within the liquid droplet. As confirmed by experiments, it modifies drastically their reaction with the surrounding atmosphere.

Besides, sophisticated measuring set-ups allowing one to follow droplet flattening and cooling as well as 3-D transient models, including solidification during flattening, have allowed a much better understanding of the splat formation and resulting crystalline structure

The weak point of coating measurements and modeling is that related to splat layering and coating formation. Simplified models are needed to understand what is impossible to follow by measuring techniques. However, reliable relationships between the particle microscopic parameters at impact, surface preparation and oxidation, temperature control before (preheating), during and after (cooling) spraying and thermomechanical properties of coatings are still missing.

REFERENCES

[1] Thermal Spraying, American Welding Society, Miami, FL, USA, 1985, p. 181.

[2] Pawlowski L., The Science and Engineering of Thermal Spray Coatings, Wiley, New York, 1995, p. 414.

[3] Boulos M.I., J. Thermal Spray Technol. 1 (1) (1991) 33–48.

[4] Freslon A., Plasma spraying at controlled temperature and atmosphere, in: Berndt C.C., Sampath S. (Eds.), Thermal Spray Science and Technology, ASM International, Materials Park, OH, USA, 1995, pp. 57–63.

[5] Meyer P.J., Hawley D., Electro plasma inc. LPPS production systems, in: Bernecki T.F. (Ed.), Thermal Spray Coatings: Properties, Processes and Applications, ASM International, Materials Park, OH, USA, 1991, pp. 29–38.

[6] Vardelle A., Vardelle M., Fauchais P., Gobin D., Monitoring particle impact on a substrate during plasma spray process, NATO Series E: Applied Science 282 (1995).

[7] Thorpe M.L., Advanced Materials and Processes 3 (1993) 50–61.

[8] Pfender E., Electric arcs and arc gas heaters, in: Hirsh M., Oskam H. (Eds.), Gaseous Electronics, Vol. 1, Academic Press, New York, 1978.

[9] Zhukov M.F., Linear direct current plasma torches, in: Sololenko O.P., Zhukov M.F. (Eds.), Thermal Plasma and New Materials Technology, Vol. 1, Cambridge Interscience, 1994, pp. 1–43.

[10] Duan Z., Wittmann K., Coudert J.F., Heberlein J., Fauchais P., in: Hrabovsky M., Konrad M., Kopecky V. (Eds.),

ISPC 14 Proc., Institute of Plasma Physics AS, CR 1 (1999) 233–238.

[11] Coudert J.F., Fauchais P., Annals of the New York Academy of Sciences 891 (1999) 382–390.

[12] Duan Z., Bell L., Planche M.P., Heberlein J., Pfender E., Stackiwicz M., in: Berndt C.C. (Ed.), Proceedings of the First United Thermal Spray Conferences, ASM International, Materials Park, OH, USA, 1997, pp. 15–18.

[13] Duan Z., Heberlein J., Janisson S., Wittmann K., Coudert J.F., Fauchais P., Effects of nozzle fluid dynamics on the dynamic characteristics of a plasma spray torch, in: Lugscheider E. (Ed.), United Thermal Spray Conference Proc., ASM International, Materials Park, OH, USA, 1999, pp. 247–252.

[14] Dorier J.L., Hollenstein C., Salito A., Loch M., Barbezat G., Influence of external parameters on arc fluctuations in a F4 DC plasma torch used for thermal spraying, in: Berndt C.C. (Ed.), ITSC 2000 Proc., ASM International, Materials Park, OH, USA, 2000, pp. 37–43.

[15] Brilhac J.F., Pateyron B., Coudert J.F., Fauchais P., Bouvier A., Plasma Chem. Plasma Process. 15 (1) (1995) 256–277.

[16] Coudert J.F., Planche M.P., Fauchais P., Plasma Chem. Plasma Process. 18 (1998) 263–283.

[17] Coudert J.F., Planche M.P., Fauchais P., Plasma Chem. Plasma Process. 16 (1) (1996) 211S–228S.

[18] Zierhut J., Haslbeck P., Landes K.D., Barbezat G. et al., in: Coddet C. (Ed.), Thermal Spray: Meeting the Challenges of the 21st Century, ASM International, Materials Park, OH, USA, 1988, pp. 1375–1379.

[19] Fauchais P., Coudert J.F., Vardelle M., Vardelle A., Denoirjean A., J. Thermal Spray Technol. 1 (2) (1992) 117–128.

[20] Fauchais P., Coudert J.F., Vardelle M., Diagnostics in thermal plasma processing, in: Auciello O., Flamm D.L. (Eds.), Plasma Diagnostics, Vol. 1, New York, Academic, 1989, pp. 349–446.

[21] Soucy G., Jurewicz J.W., Boulos M.I., Plasma Chem. Plasma Process. 15 (4) (1995) 693–710.

[22] Rahmane M., Soucy G., Boulos M.I., Plasma Chem. Plasma Process. 16 (1) (1996) 169S–190S.

[23] Snyder S.C., Reynolds L.D., Fincke J.R., Lassahn G.D., Grandy J.D., Repetti T.E., Phys. Rev. E 50 (1994) 519–529.

[24] Pfender E., Fincke J.R., Spores R., Plasma Chem. Plasma Process. 1 (4) (1991) 529–544.

[25] Coudert J.F., Planche M.P., Fauchais P., Plasma Chem. Plasma Process. 15 (1) (1994) 639–652.

[26] Coudert J.F., Planche M.P., Fauchais P., Plasma Chem. Plasma Process. 16 (1) (1995) 47–69.

[27] Hoffman T., Advanced Materials and Processes 140 (3) (1991) 37–43.

[28] Duan Z., Heberlein J., Anode boundary layer effects in plasma spray torches, in: Berndt C.C. (Ed.), ITSC 2000 Proc., ASM International, Materials Park, OH, USA, 2000, pp. 1–7.

[29] Lagnoux O., Coudert J.F., Wittmann K., Fauchais P., Study of the air entrainment within d.c. plasma jets, in: Berndt C.C. (Ed.), ITSC 2000 Proc., ASM International, Materials Park, OH, USA, 2000, pp. 71–77.

[30] Boulos M., Fauchais P., Pfender E., Thermal Plasmas Fundamentals and Applications, Vol. 1, Plenum Press, New York/London, 1994, p. 452.

[31] André P., Abbaoui M., Lefort A., Pariset M.J., Plasma Chem. Plasma Proc. 16 (3) (1996) 379–398.

[32] Pateyron B., Elchinger M.F., Delluc G., Fauchais P., Plasma Chem. Plasma Proc. 16 (1) (1996) 39–57.

[33] Murphy B., High Temp. Material Processes 4 (2000) 1–20.

[34] Snyder S.C., Murphy A.B., Hofeldt D.L., Reynolds L.D., Phys. Rev. E 52 (3) (1995) 2999–3009.

[35] Murphy A.B., Phys. Rev. E 55 (6) (1997) 7473–7494.

[36] Libermann R.W., Lowke J.J., J. Quant. Spectrosc. Radiat. Transfer 16 (1976) 253–260.

[37] Gleizes A., Gonzalez J.J., Liani B., Rahmani B., J. de Physique 51 (C5) (1990) 213–219.

[38] Erraki A., Naghizadeh-Kashani N., Cressault Y., Gleizes A., Determination of radiative transfer in thermal plasmas, in: Hrabovsky M., Konrad M., Kopexky V. (Eds.), ISPC 14 Proc., Inst. of Phys. AS, CR 1 (1999) 337–342.

[39] Cressault Y., Gleizes A., Radiative and transport properties in Ar–H_2–Cu mixtures at atmospheric pressure, in: Proc. of TPP6 (accepted, to be published by Begell House, New York).

[40] Elchinger M.F., Pateyron B., Fauchais P., Vardelle A., Calculation of thermodynamic and transport properties of Ar–H_2–Air plasma, comparison with simple mixing rules, in: Wu C.K. (Ed.), 13th International Symposium on Plasma Chemistry, Proceedings Supplement, Beijing, China, Peking University Press, 1997, pp. 1997–2003.

[41] Rat V., André P., Aubreton J., Elchinger M.F., Fauchais P., Lefort A., Calculation of combined diffusion coefficients from the simplified theory of transport properties, in: Proc. of TPP6 (accepted, to be published by Begell House, New York).

[42] Potapov A.V., High Temp. 4 (1966) 48–51.

[43] Van de Sanden M.C.M., Schram P.P.J.M., Peeters A.G., van der Mullen J.A.M., Kroesen G.M.W., Phys. Rev. A 40 (9) (1989) 5273–5276.

[44] Cliteur G.J., Suzuki K., Tanaka Y., Sakuta T., Matsubara T., Yokomizu Y., Matsumura T., J. Phys. D 32 (1999) 1851–1856.

[45] Girard R., Belhouari J.B., Gonzalez J.J., Gleizes A., J. Phys. D 32 (1999) 2890–2901.

[46] Andre P., Aubreton J., Elchinger M.F., Lefort P., A new modified pseudo-equilibrium calculation to determine the composition of hydrogen and nitrogen plasmas at atmosphere pressure, Plasma Chem. Plasma Proc. (accepted).

[47] Heberlein J., Electrode phenomena in plasma torches, in: Fauchais P., van der Mullen J., Heberlein J. (Eds.), Heat and Mass Transfer Under Plasma Conditions, Annals of the New York Academy of Sciences 891 (1999) 14–27.

[48] Delalondre C., Zahrai S., Simonin O., in: Fauchais P., (Ed.), Heat and Mass Transfer Under Thermal Plasma Conditions, Begell House, New York, USA, 1995, pp. 1–14.

[49] Chyou Y.P., Pfender E., Plasma Chem. Plasma Proc. 9 (1989) 291–307.

[50] Huang P.C., Heberlein J., Pfender E., Plasma Chem. Plasma Proc. 15 (1995) 25–37.

[51] Bouvier A., Delalondre C., Simonin O., Brilhac J.F., Numerical modeling of the internal behavior of a vortex stabilized plasma torch, in: Fauchais P., Boulos M., van der Mullen J. (Eds.), Heat and Mass Transfer under Thermal Plasma Conditions, Begell House, New York, USA, 1995, pp. 79–89.

[52] Murphy A.B., Kovitya P., J. Appl. Phys. 73 (1993) 4759–4767.

[53] Paik S., Huang P.C., Heberlein J., Pfender E., Plasma Chem. Plasma Proc. 13 (1993) 103–128.

[54] Kaddani A., Zaharai S., Delalondre C., Simonin O., J. Phys. D 28 (1995) 2294–2302.

[55] El-Kaddah N., McKelliget J., Szekely J., Met. Trans. B 15B (1984) 59–70.

[56] Scott D.A., Kovitya P., Haddad G.N., J. Appl. Phys. 66 (11) (1989) 5232–5240.

[57] Dilawari A.H., Szekely J., Westhoff R., Plasma Chem. Plasma Proc. 10 (4) (1990) 501–520.

[58] Westhoff R., Trapaga G., Szekely J., Met. Trans. B 29B (1992) 683–693.

[59] Ramshaw J.D., Chang C.H., Plasma Chem. Plasma Proc. 12 (3) (1992) 299–325.

[60] Chang C.H., Ramshaw J.D., Phys. Plasmas 1 (1994) 3698–3708.

[61] Chang C.H., Ramshaw J.D., Plasma Chem. Plasma Proc. 16 (1996) 5S–17S.

[62] Dussoubs B., Fauchais P., Vardelle A., Vardelle M., Themelis N.J., Computational analysis of a three-dimensional plasma spray jet, in: Berndt C.C. (Ed.), Thermal Spray: A United Forum for Scientific and Technological Advances, ASM International, Materials Park, OH, USA, 1997, pp. 557–565.

[63] Pfender E., Chang C.H., Plasma spray jets and plasma particulate interactions: modeling and experiment, in: Coddet C. (Ed.), Proc. of ITSC 98, ASM International, Materials Park, OH, USA, 1998, pp. 315–327.

[64] Brossa M., Pfender E., Plasma Chem. Plasma Proc. 8 (1988) 75–93.

[65] Spalding D.B., Int. J. Physicochem. Hydrodynam. 4 (1983) 323–332.

[66] Huang P.C., Heberlein J., Pfender E., Plasma Chem. Plasma Proc. 15 (1995) 25–46.

[67] Vardelle M., Vardelle A., Dussoubs B., Fauchais P., Roemer T.J., Neiser R.A., Smith M.F., Influence of injector geometry on particle trajectories: Analysis of particle dynamics in the injector and plasma jet, in: Coddet C. (Ed.), Thermal Spray: Meeting the Challenges of the 21st Century, ASM International, Materials Park, OH, USA, 1998, pp. 887–894.

[68] Kubel J., Jr., Advanced Materials and Processes 12 (1990) 24–32.

[69] Kolman B., Forman J., Dubsky J., Chraska P., Mikrochim. Acta 114/115 (1194) 335–342.

[70] Wigren J., de Vries J.F., Greving D., Effects of powder morphology, microstructure, and residual stresses on thermal barrier coating thermal shock performance, in: Berndt C.C. (Ed.), Thermal Spray: Practical Solutions for Engineering Problems, ASM International, Materials Park, OH, USA, 1996, pp. 855–861.

[71] Anderson I.E., Sordelet D.J., Besser M.F. and Terpstra R.L., Effects of powder morphology on pneumatic feeding and plasma spray deposition, in: Coddet C. (Ed.), Proceedings of the 15th International Thermal Spray Conference, Vol. 1, ASM International, Materials Park, OH, USA, 1999, pp. 911–916.

[72] Vardelle A., Themelis N.J., Dussoubs B., Vardelle M., Fauchais P., Transport and chemical rate phenomena in plasma sprays, J. High Temp. Chem. Proc. 1 (3) (1997) 295–314.

[73] Zhang H., Espie G., Themelis N.J., Vardelle A., Vardelle M., Oxidation and evaporation of iron droplets in a plasma jet, in: 14th International Symposium on Plasma Chemistry, Symposium Proceedings, Prague, 2–6 August 1999, pp. 2775–2285.

[74] Vardelle A., Baronnet J.M., Vardelle M., Fauchais P., IEEE Transactions on Plasma Sciences 8 (1980) 418.

[75] Fincke J.R., Swank W.D., Jeffery C.L., Mancuso C.A., Meas. Sci. Technol. 4 (1993) 559.

[76] Sakuta T., Boulos M.I., Rev. Sci. Instrum. 59 (1988) 285.

[77] Smith M.F., O'Hern T.J., Brockman J.E., Neiser R.A., in: Berndt C.C. (Ed.), Thermal Spray Science and Technology, ASM International, Materials Park, OH, USA, 1995, pp. 105–111.

[78] Moreau C., Gougeon P., Burgess A., Ross D., in: Berndt C.C. (Ed.), Thermal Spray Science and Technology, ASM International, Materials Park, OH, USA, 1995, pp. 141–147.

[79] Léger A.C., PhD Thesis, n° 4-97, University of Limoges, France, 1997.

[80] Bourque G., Lamontagne M., Moreau C., in: Berndt C.C. (Ed.), Thermal Spray Surface Engineering via Applied Research, ASM International, Materials Park, OH, USA, 2000, pp. 45–51.

[81] Li K.-I., Vardelle M., Fauchais P., in: Berndt C.C. (Ed.), Advances in Thermal Spray Science and Technology, ASM International, Materials Park, OH, USA, 1995, pp. 45–51.

[82] Vattulainen J., Knuuttila J., Lehtinent T., Mantyla T., Hernberg R., in: Coddet C. (Ed.), Proceedings of the 15th International Thermal Spray Conference, Vol. 1, ASM International, Materials Park, OH, USA, 1998, pp. 667–672.

[83] Moreau C., in: Coddet C. (Ed.), Proceedings of the 15th International Thermal Spray Conference, Vol. 2, ASM International, Materials Park, OH, USA, 1998, pp. 1681–1691.

[84] Li K-I., Vardelle M., Vardelle A., Fauchais P., Trassy C., Vaporization of metal powders in plasma sprays, in: Berndt C.C. (Ed.), Practical Solutions for Engineering Problems, ASM International, Materials Park, OH, USA, 1996, pp. 547–552.

[85] Pfender E., Particle behavior in thermal plasmas, Plasma Chem. Plasma Proc. 9 (1) (1989) 167S–194S.

[86] Boulos M., Fauchais P., Vardelle A., Pfender E., Fundamentals of plasma particle momentum and heat transfer, in: Suryanarayanan R. (Ed.), Plasma Spraying, World Scientific, Singapore, 1993, pp. 3–71.

[87] Bourdin E., Fauchais P., Boulos M.I., Transient heat conduction under plasma conditions, Int. J. Heat Mass Trans. 26 (4) (1983) 567–582.

[88] Williamson R.L., Fincke J.R., Chang C.H., A computational examination of the sources of statistical variance in particle parameters during thermal plasma spraying, Plasma Chem. Plasma Proc. 20 (3) (2000).

[89] Jones, Rep. Prog. Phys. 36 (1973) 1425.

[90] Wang G.X., Matthys E.F., International Journal of Rapid Solidification 6 (1991) 297.

[91] Clyne T.W., Met. Trans. B 15B (1994) 369–381.

[92] Clyne T.W., Gill S.C., J. Thermal Spray Technol. 5 (1996) 401–418.

[93] Kuroda S., Properties and characterization of thermal sprayed coatings. A review of recent research progress, in: Coddet C. (Ed.), Thermal Spray: Meeting the Challenges of the 21st Century, ASM International, Materials Park, OH, USA, 1998, pp. 539–550.

[94] Houben J.M., Ph.D. Thesis, Technishe Universiteit Eindhoven, Eindhoven, Netherlands, 1988.

[95] Dykhuisen R.C., J. Thermal Spray Technol. 3 (1994) 351–371.

[96] Fauchais P., Vardelle M., Vardelle A., Bianchi L., in: Vincenzini P. (Ed.), Advances in Inorganic Films and Coatings, 1995, Techna Faenze, Italy, pp. 83–97.

[97] Jiang X., Matejicek J., Sampath S., Materials Science and Engineering A272 (1999) 189.

[98] DPV-2000, Tecnar Automation Ltee, St. Hubert, Quebec, Canada.

[99] Spraywatch, Oseir Ltd., Tempere, Finland.

[100] Moreau C., Cielo P., Lamontagne M., Dallaire S., Vardelle M., Meas. Sci. Technol. 1 (1990) 807–815.

[101] Moreau C., Gougeon P., Lamontagne M., J. Thermal Spray Technol. 4 (1) (1995) 25–33.

[102] Gougeon P., Moreau C., in: Berndt C.C. (Ed.), Thermal Spray: A United Forum for Scientific and Technological Advances, ASM International, Materials Park, OH, USA, 1997, pp. 619–625.

[103] Vardelle M., Vardelle A., Fauchais P., Moreau C., Meas. Sci. Technol. 5 (1994) 205–212.

[104] Leger A.C., Vardelle M., Vardelle A., Fauchais P., Sampath S., Berndt C.C., Herman H., in: Berndt C.C. (Ed.), Thermal Spray: Practical Solutions for Engineering Problems, ASM International, Materials Park, USA, 1996, pp. 623–629.

[105] Escure C., Vardelle M., Fauchais P., in: Berndt C.C. (Ed.), Proc. Int. Thermal Spray Conference, ASM International, Materials Park, OH, USA, 2000, pp. 743–752.

[106] Madjeski J., Int. J. Heat Mass Trans. 26 (1983) 1095–1098.

[107] Fiedler R., Naber J., in: Proc. of Combustion Institute Spring Technical Meeting on Combustion Fundamentals and Applications, 1989, p. 269.

[108] Bennett T., Poulikakos D., J. Mat. Sci. 28 (1993) 961–970.

[109] Trapaga G., Szekely J., Met. Trans. B 22B (1991) 901–914.

[110] Liu H., Lavernia E.J., Rangel R.H., J. Phys. D 26 (1993) 1900–1908.

[111] Pasendideh-Fard M., Mostaghimi J., in: Berndt C.C. (Ed.), Proc. of the 7th National Thermal Spray Conference, ASM International, Materials Park, OH, USA, 1994, pp. 405–411.

[112] Bertagnoli M., Marchese M., Jaccuci G., Doltsinis I., Noelting S., J. Comp. Phys. 133 (1997) 205–216.

[113] Montavon G., Feng Z.G., Coddet C., Feng Z.Q., Domaszewski M., in: Berndt C.C. (Ed.), Thermal Spray: A United Forum for Scientific and Technological Advances, ASM International, Materials Park, OH, USA, 1997, pp. 627–633.

[114] Bussmann M., Aziz S.D., Chandra S., Mosthagimi J., in: Coddet C. (Ed.), Thermal Spray: Meeting the Challenges of the 21st Century, ASM International, Materials Park, OH, USA, 1998, pp. 413–418.

[115] Vardelle A., Vardelle M., Fauchais P., Gobin D., NATO Series E: Applied Science 282 (1995) 95–121.

[116] Robert C., Vardelle A., Wang G. X., Sampath S., in: Coddet C. (Ed.), Thermal Spray: Meeting the Challenges of the 21st Century, ASM International, Materials Park, OH, USA, 1998, pp. 729–734.

[117] Vardelle M., Vardelle A., Léger A.C., Fauchais P., Gobin D., J. Thermal Spray Technol. 4 (1) (1995) 50–58.

[118] Fukumoto M., Huang Y., Ohtawari M., in: Coddet C. (Ed.), Thermal Spray: Meeting the Challenges of the 21st Century, ASM International, Materials Park, OH, USA, 1998, pp. 401–407.

[119] Li C., Li J.L., Wang W.B., Sampath S., in: Coddet C. (Ed.), Thermal Spray: Meeting the Challenges of the 21st Century, ASM International, Materials Park, OH, USA, 1998, pp. 473–479.

[120] Jiang X., Wan Y., Herman H., Sampath S., Fragmentation of impinging molten ZrO_2 droplets on substrate during thermal spray (1999) (submitted for publication).

[121] Huang Y., Ohwatari M., Fukumoto M., in: Proc. of the 6th Int. Sympos. of the Japan Welding Society, 1996, pp. 731–737.

[122] Fauchais P., Leger A.C., Vardelle M., Vardelle A., Formation of plasma sprayed oxide coatings, in: Apelian D., Avans J.W., Sohu H.Y. (Eds.), Proc. of the Julian Szekely Symposium Materials Processing, TMS, USA, 1997, pp. 571–592.

[123] McPherson R., Thin Solid Films 83 (1981) 297–310.

[124] Kuroda S., Dendo T., Kitahara S., J. Thermal Spray Technol. 4 (1) (1995) 75–84.

[125] Pech J., Hannoyer B., Denoirjean A., Fauchais P., Influence of substrate preheating monitoring on alumina splat formation in d.c. plasma processes, in: Berndt C.C. (Ed.), ITSC 2000 Proc., ASM International, Materials Park, OH, USA, 2000, pp. 759–765.

[126] Bianchi L., Grimaud A., Blein F., Lucchese P., Fauchais P., J. Thermal Spray Technol. 4 (1) (1995) 59–66.

[127] Lin C.K., Berndt C.C., J. Thermal Spray Technol. 3 (1) (1994) 75–104.

[128] Renault T., Vardelle M., Grimaud A., Fauchais P., Hoffman H., On-line control of particle spray jet and residual stresses in plasma sprays, in: Berndt C.C. (Ed.), ITSC 2000 Proc., ASM International, Materials Park, OH, USA, 2000, pp. 1383–1391.

[129] Brandt O., Wandelt M., Thermal measurements of substrate during spray processes, in: Berndt C.C. (Ed.), Thermal Spray: Practical Solutions for Engineering Problems, ASM International, Materials Park, OH, USA, 1996, pp. 799–802.

[130] Lugscheider E., Ladru F., Gourlaven V., Gualco C., Enhanced atmospheric plasma spraying of thick TBCs by improved process control and deposition efficiency, in: Coddet C. (Ed.), Thermal Spray: Meeting the Challenges of the 21st Century, Vol. 2, ASM International, Materials Park, OH, USA, 1998, pp. 1583–1588.

[131] Jokinen P., Varis T., Korpiola K., Kauppinen, In-situ temperature control of coating and workpiece in thermal spraying, in: Lugscheider E. (Ed.), UTSC 1999 Proc., ASM International, Materials Park, OH, USA, 1999, pp. 318–320.

[132] Lugscheider E., Ladru F., Crostack H.-A., Reuss G., Haubold T., On-line process monitoring during spraying of TBCs by acoustic emission, in: Lugscheider E. (Ed.), UTSC 1999 Proc., ASM International, Materials Park, OH, USA, 1999, pp. 312–317.

[133] Leger A.C., Grimaud A., Fauchais P., Delluc G., Influence of the torch to substrate velocity and resulting temperature on the residual stresses in alumina plasma sprayed coatings, in: Berndt C.C. (Ed.), Thermal Spray: A United Forum for Scientific and Technological Advances, ASM International, Materials Park, OH, USA, 1997, pp. 823–829.

[134] Leger A.C., Haddadi A., Pateyron B., Delluc G., Grimaud A., Nardou F., Fauchais P., Residual stresses during coating generation: plasma sprayed alumina coating on XC 38, measurements and calculations, in: Coddet C. (Ed.), Thermal Spray: Meeting the Challenges of the 21st Century, ASM International, Materials Park, OH, USA, 1998, pp. 895–903.

[135] Tsui Y.C., Clyne T.W., An analytical model for predicting residual stresses in progressively deposited coatings onto planar geometries, in: Berndt C.C. (Ed.), NTSC 97, ASM International, Materials Park, OH, USA, 1997, pp. 813–822.

[136] Leger A.C., Grimaud A., Fauchais P., Catteau C., New set-up to measure residual stresses during plasma sprayed coating formation and cooling, in: Berndt C.C. (Ed.), Thermal Spray: Practical Solutions for Engineering Problems, ASM International, Materials Park, OH, USA, 1996, pp. 891–896.

[137] Liao H., Vaslin P., Yang Y., Coddet C., J. Thermal Spray Technol. 6 (2) (1997) pp. 235–241.

[138] Bianchi L., Baradel N., Llorca-Isern N., Bertran-Vidal G., Influence of plasma spraying parameters on coating damage, in: Berndt C.C. (Ed.), ITSC 2000 Proc., ASM International, Materials Park, OH, USA, 2000, pp. 29–36.

[139] Swank W.D., Gavalya R.A., Wright J.K., Wright R.N., Residual stress determination from a laser-based curvature measurement, in: Berndt C.C. (Ed.), ITSC 2000 Proc., ASM International, Materials Park, OH, USA, 2000, pp. 363–369.

[140] Zhang T., Qiu Z., Bao Y., Gawne D.T., Zhang K., Temperature profiles and thermal stress analysis of plasma sprayed glass-composite coatings, in Berndt C.C. (Ed.), ITSC 2000 Proc., ASM International, Materials Park, OH, USA, 2000, pp. 355–361.

[141] Haddadi A., Elaboration by plasma spraying of zirconia and alumina coatings: Columnar growth, residual stresses and modeling, Ph.D. Thesis, University of Limoges, France, 1998.

[142] Fauchais P., Vardelle M., Vardelle A., Pateyron B., Effets thermiques sur la construction des dépôts de céramiques oxides projetées par plasma, in: Proceedings of the Congrès SFT 1999 (to be published).

[143] Monerie-Moulin F., Gitzhofer F., Fauchais P., Boulos M.I., Vardelle A., J. High Temperature Chemical Processes 1 (3) (1992) 249–257.

[144] Haddadi A., Grimaud A., Denoirjean A., Nardou F., Fauchais P., Crystalline growth within alumina and zirconia coatings with coating temperature control during spraying, in: Berndt C. (Ed.), Thermal Spray: Practical Solutions for Engineering Problems, ASM International, Materials Park, OH, USA, 1996, pp. 615–622.

[145] ABAQUS, User's manual, Version 5–6, Hibbit, Karlsson, Sorenson, Pawtucket, RI, 1996.

[146] Nissley D.M., J. Thermal Spray Technol. 6 (1) (1997) 91–98.

[147] Kerkhoff G., Vassen R., Stöver D., Numerically calculated thermal stresses in thermal barrier coatings on cylindrical substrates, in: Lugscheider E. (Ed.), ITSC 1999 Proc., ASM International, Materials Park, OH, USA, 1999, pp. 787–792.

[148] Lugscheider E., Ladru F., Gourlaouen V., Gualco C., Enhanced atmospheric plasma spraying of thick TBCs by improved process control and deposition efficiency, in: Coddet C. (Ed.), Thermal Spray: Meeting the Challenges of the 21st Century, ASM International, Materials Park, OH, USA, 1998, pp. 1583–1588.

[149] Nylen P., Fransson I., Wretland A., Martensson N., Coating thickness prediction and robot trajectory generation of thermal sprayed coatings, in: Berndt C. (Ed.), Thermal Spray: Practical Solutions for Engineering Problems, ASM International, Materials Park, OH, USA, 1996, pp. 693–698.

[150] Vivekanandahn T., Kashani A.R., Echenpati R., J. Thermal Spray Technol. 3 (2) (1994) 208–218.

[151] Bonnet R., Bolot R., Coddet C., Simulation of the thermal spray process and off-line programming, in: Lugscheider E., Kammer P.A. (Eds.), Proceedings of United Thermal Spray Conference, ASM International, Materials Park, OH, USA.

[152] Hansbo A., Nylen P., Surface and Coatings Technology 122 (2–3) (1999) 190–200.

[153] Montillet D., Dombre E., Valentin P., Goubot J.M., Modeling, simulating and optimizing the robotized plasma deposition: air experimental approach, in: Lugscheider E. (Ed.), UTS 1999, ASM International, Materials Park, OH, USA, 1999, pp. 507–512.

[154] Hansbo A., Nylen P., Modeling of spray deposition and robot motion, optimization for a gas turbine application, in: Berndt C. (Ed.), ITSC 2000 Proc., ASM International, Materials Park, OH, USA, 2000, pp. 203–209.

[155] Knotek O., Elsing R., Monte-Carlo simulation of the lamellar structure of thermally sprayed coatings, Surface Coating Technology 32 (1987) 261–271.

[156] Fukanuma H., J. Thermal Spray Technol. 3 (1) (1994) 33–44.

[157] Pekshev P.Yu., Murzin I.G., Surf. Coating Technology 56 (1993) 199–208.

[158] Cirolini S., Harding J.H., Jacucci G., Surf. Coating Technology 48 (1991) 137–145.

[159] Harding J.H., Mulheran R.A., Cirolini S., Marchese M., Jacucci G., J. Thermal Spray Technol. 4 (1) (1995) 34–39.

[160] Ahmad I., Bergneau T.L., J. Thermal Spray Technol. 8 (2) (1999) 315–322.

[161] Pasandideh-Fard M., Mostaghini J., Chandra S., Numerical simulation of thermal spray coating formation, in: Berndt C.C. (Ed.), ITSC 2000 Proc., ASM International, Materials Park, OH, USA, 2000, pp. 125–133.